Identification of α-Fe in high-silica zeolites based on ab initio electronic structure calculations

Simon D. Hallaert,[†] Max L. Bols,[‡] Pieter Vanelderen,[‡,¶] Robert A. Schoonheydt,[‡] Bert F. Sels,[‡] and Kristine Pierloot[*,†]

†*Department of Chemistry, KU Leuven, Celestijnenlaan 200F, B-3001 Leuven, Belgium*

‡*Centre for Surface Chemistry and Catalysis, KU Leuven, Celestijnenlaan 200F, B-3001 Leuven, Belgium*

¶*Current address: IMEC, Kapeldreef 75, B-3001 Heverlee, Belgium*

E-mail: kristin.pierloot@kuleuven.be

Abstract

α-Fe is the precursor of the reactive Fe(IV)=O core responsible for methane oxidation in Fe-containing zeolites. To get more insight into the nature and stability of α-Fe in different zeolites, the binding of Fe(II) at six-membered cation exchange sites (6MR) in ZSM-5, zeolite beta and ferrierite was investigated using DFT and multi reference ab initio methods (CASSCF/CASPT2). CASPT2 ligand field (LF) excitation energies of all sites were compared with the experimental DR-UV-vis spectra reported by Snyder et al. [*Nature*, 536 (7616):317–321, 2016] . From this comparison it is concluded that the 16 000 cm^{-1} band of α-Fe, observed in all three zeolites, can uniquely be assigned to a high spin square planar (SP) Fe(II) located at a 6MR with Al-Si-Si-Al sequence, where the Al are positioned opposite in the ring and as close to each other as possible. The stability of such conformations is also confirmed by the binding energies obtained from DFT. The bands at 10 000 cm^{-1} in the experimental spectra, assigned to spectator Fe(II), are attributed to six coordinated trigonal prismatic Fe(II) species, as calculated for the γ-site in ZSM-5. The entatic effect of the zeolite lattice on the stability of the SP sites was investigated making use of an unconstrained Fe(II) model complex FeL_2 (with L = $[Al(OH)_4]^-$). The SP conformer is approximately 2 kcal/mol more stable than the tetrahedral one, indicating that the SP coordination environment of α-Fe is not imposed by the zeolite lattice but rather electronically preferred by Fe(II) in the environment of four O ligands. A significant contribution to the stability of the SP conformer is provided by mixing of the doubly occupied $3d_{z^2}$ orbital with the higher lying 4s.

Introduction

A wide variety of metalloenzymes, such as the family of P450 enzymes,[1,2] the non-heme iron enzyme soluble methane monooxygenase (sMMO)[3] and many others, catalyzes hydroxylation of the unreactive C-H bond on several different substrates in a very efficient way. Inspired by this success, scientist are extensively searching for model complexes that mimic these reactions. However, most of such model complexes have a reactivity that is much lower when compared to the reactivity of real enzymes.[4] An interesting exception is formed by Fe-containing zeolites. More than 20 years ago, Panov and coworkers described the selective oxidation of methane to methanol and benzene to phenol at room temperature over Fe-ZSM-5.[5,6] The remarkable reactivity was attributed to an Fe-oxygen species formed from an oxygen abstraction by its Fe(II) precursor, called α-O and α-Fe respectively. In the last decades, this reaction has been intensively studied both experimentally[7–12] and theoretically.[13–18] However, despite a large body of research, the exact nature of α-O and α-Fe is a matter of longstanding debate. This is mainly because α-O and α-Fe are minority species amongst different spectator species in the zeolite, making data from bulk spectroscopic techniques such as X-ray absorption spectroscopy and reactivity studies difficult to interpret.[19,20]

The problem of the spectator species was circumvented in a recent study by Snyder et al.[21] They used a site selective spectroscopic method, i.e. variable temperature variable field Magnetic Circular Dichroism (VTVH-MCD), to selectively identify spectroscopic features in the Diffuse Reflectance (DR) ligand field spectrum of α-O and α-Fe in zeolite Beta (framework type *BEA). In combination with DFT and ab initio (CASPT2) calculations, this approach resulted in an unambiguous identification of α-Fe as a mononuclear, high spin (S=2), square planar Fe(II) species and α-O as a mononuclear, high spin (S=2), square pyramidal Fe(IV)=O species, both located at a six-membered ring (6MR), called β-site, in *BEA.[21] The CASPT2 results indicated that the band at 15 900 cm^{-1} in the DR spectrum of α-Fe could be attributed to a $d_{z^2} \rightarrow d_{x^2-y^2}$ transition.[21] Similar α-Fe bands were observed at 15 200 cm^{-1} in ZSM-5 (framework type MFI) and 16 100 cm^{-1} in ferrierite (framewor

type FER), two other zeolites that are known to contain α-Fe(II).[21] However, in contrast to *BEA, ZSM-5 and FER have several cation exchanges sites containing 6MRs. This raises the question which of these sites might be able to accommodate Fe(II) in a square planar fashion, thus creating α-Fe similar as in zeolite *BEA. In this work, we aim to provide a decisive answer to this question by means of a thorough computational study of Fe(II) species at several cation exchange sites in ZSM-5, *BEA and FER. Density functional theory (DFT) is used to obtain the optimal structure and binding energy of Fe(II) at different 6MRs, while a theoretical estimate of the d-d excitation energies at these sites is obtained by means of multiconfigurational second-order perturbation theory (CASPT2) and compared to the experimental LF spectra.

As was also discussed in ref. 21, the square planar coordination environment of α-Fe is very convenient with respect to its role as precursor for the active α-O species. Indeed, activation of square planar α-Fe results in a square pyramidal ^{5}Fe(IV)=O species with an empty coordination site *trans* to the O ligand. DFT calculations were used to show that the zeolite environment at the α-O site governs the reactivity for O–H bond formation in two aspects, that is (a) by denying the ^{5}Fe(IV)=O species a sixth ligand at it *trans* axial position, and (b) by enforcing its square pyramidal (rather than trigonal bipyramidal) structure. Both factors serve to destabilize ^{5}Fe(IV)=O relative to the ^{6}Fe–OH reaction product by several kcal/mol, thus increasing the driving force for O–H bond formation by the same amount. This points to a well-defined 'entatic' state for α-O governed by its zeolite environment.[22] It remains, however, unclear to what extent the zeolite also plays a determining role in the square planar structure of the α-Fe precursor, in the sense that it would force the Fe(II) into a 'strained' geometry. This question is highly relevant,[23] because high spin square planar Fe(II) complexes are rare in coordination chemistry and were originally only observed in solid state environments similar to zeolites, such as minerals and ceramics,[24–26] where their unusual square planar (rather than tetrahedral) geometry was indeed attributed to constraints by the crystal lattice. More recently, however, a number of molecular compounds containing

high-spin square planar FeL_4 arrangements in a non-strained environment were presented, suggesting that specific ligand environments may inherently electronically stabilize a square planar over a tetrahedral structure.[27–31] In ref. 27 the preference for a square planar structure was rationalized with the help of DFT calculations, as a Jahn-Teller (JT) flattening of the usual FeL_4 tetrahedron, caused by four highly charged, π-basic ligands L. In the present work this explanation will be further explored in the specific context of α-Fe in a zeolite environment, making use of a combined DFT/CASPT2 approach.

Experimental details

Preparation of Fe-zeolites

Fe-ZSM-5 (having MFI topology), Fe-beta (*BEA) and Fe-ferrierite (FER) zeolites were prepared from the corresponding dehydrated acid zeolites by diffusion impregnation of $Fe(acac)_3$ (acac = acetylacetonate) in toluene solution. The method was identical to the sample preparation in ref 21. Following impregnation, all samples were calcined in air at 550 °C to remove organic material. This preparation method minimizes Fe heterogeneity and limits the formation of oxide/hydroxide species (relative to aqueous exchange or sublimation). The samples, each approximately 1 gram, were then subjected to high-temperature treatment at 900 °C in a 30 cm^3 min^{-1} flow of helium for two hours, followed by treatment in 30 ml min^{-1} H_2 for one hour at 700°C. The Fe content of the resulting Fe(II)-zeolites was determined by inductively coupled plasma mass spectrometry. N_2O activation of Fe(II)-zeolite (1 gram) was performed at 230 °C using a 5 vol% N_2O/helium flow (30 cm^3 min^{-1}) The CH_4 reaction was performed at room temperature using a 10 vol% CH_4/helium flow (50 cm^3 min^{-1}).

Diffuse reflectance spectroscopy

DR-UV-vis spectra were recorded on a Varian Cary 5000 UV–VIS–NIR spectrophotometer at room temperature against a halon white reflectance standard in the range 4 000–50 000

cm^{-1}. All treatments before *in situ* UV-vis-NIR spectroscopic measurements were performed in a quartz U-tube/flow cell. The latter was equipped with a window for *in situ* UV-vis-NIR diffuse reflectance spectroscopy.

Computational details

Geometry optimizations

The cation exchange sites of the zeolites are in this work represented by cluster models. DFT structure optimizations of such clusters were performed with Turbomole 6.4 software[32] using the B3LYP[33–38] functional, a def2-QZVPP[39] basis set on Fe and def2-TZVP[40] basis sets on all other atoms. The cluster models were obtained by taking the cation exchange sites from the zeolites' crystal structure (vide infra).[41,42] The terminal oxygen atoms were end-capped with H atoms and were fixed during the geometry optimization, whereas H was allowed to optimize its O-H distance, but the direction of this bond was fixed. Fe was then placed in the ring and a new structure optimization was performed on the quintet surface, keeping the terminal O and H atoms fixed.

In order to compensate for the (+2) charge of Fe(II), two Si atoms were replaced by Al in each ring. For each ring, different Al distributions were chosen. To distinguish different clusters the following notation was used: the ring structure is represented by its Greek letter and the position of Al is given between brackets. For example, β(T4T10) depicts a β-ring structure with Al on T4 and T10 positions. The numbering of T is consistent with ref. 41 for Fe-ZSM-5 and with ref. 42 for Fe-BEA and Fe-FER.

To compare the relative stability of different clusters, the binding energy (BE) for Fe(II) to the cluster was calculated as follows:

$$\mathrm{BE} = E[\mathrm{Fe(II)}] + E[\mathrm{Cluster}] - E[\mathrm{Cluster(Fe(II))}] \quad (1)$$

Due to the large electrostatic attraction between the bare Fe(II) ion and the negatively charged zeolite clusters unrealistically large binding energies are obtained from these calculations. Therefore, all discussions will be based on relative rather than absolute binding energies.

Calculation of the d-d transitions

The ligand field (LF) spectrum of Fe(II) in different clusters was calculated using state average single point CASSCF/CASPT2[43] calculations on the DFT-B3LYP optimized models, making use of the MOLCAS-7.9 software.[44] Extended ANO-RCC basis sets[45,46] were used, contracted to [7s6p5d3f2g1h] for Fe, [4s3p2d1f] for O, [4s3p1d] for Si and Al, and [2s1p] for H. A scalar-relativistic second order Douglass-Kroll Hamiltonian[47] was used and a Cholesky decomposition technique (with a threshold of 10^{-1} a.u.) was used to approximate the two-electron repulsion integrals.

CASSCF/CASPT2 calculations are performed in two steps. First, a CASSCF (complete active space SCF) reference wavefunction is built. The active space used to construct this reference wavefunction was chosen according to the standard rules for transition metal complexes,[43] i.e. five 3d and five 4d orbitals of Fe and the bonding 2p orbitals of the coordinating O atoms. Depending on the coordination environment of Fe(II) in the different clusters, this results in 8 electrons distributed over 11 orbitals CAS(8,11) for structures with a square planar and square pyramidal coordination and CAS(10,12) for structures with a trigonal prismatic coordination (vide infra). A plot of the active orbitals of the cluster containing Fe(II) at the β(T4T10) site of Fe-ZSM-5 is provided in Figure 1.

In the second step, a CASPT2 calculation is performed on the CASSCF reference wave function in order to account for the dynamical correlation contribution. In this step, all electrons except those from 1s, 2s, 2p of Fe, Si and Al and 1s of O were correlated. All CASPT2 calculations used a zeroth-order Hamiltonian with the standard IPEA shift[48] and an imaginary shift[49] of 0.1 a.u..

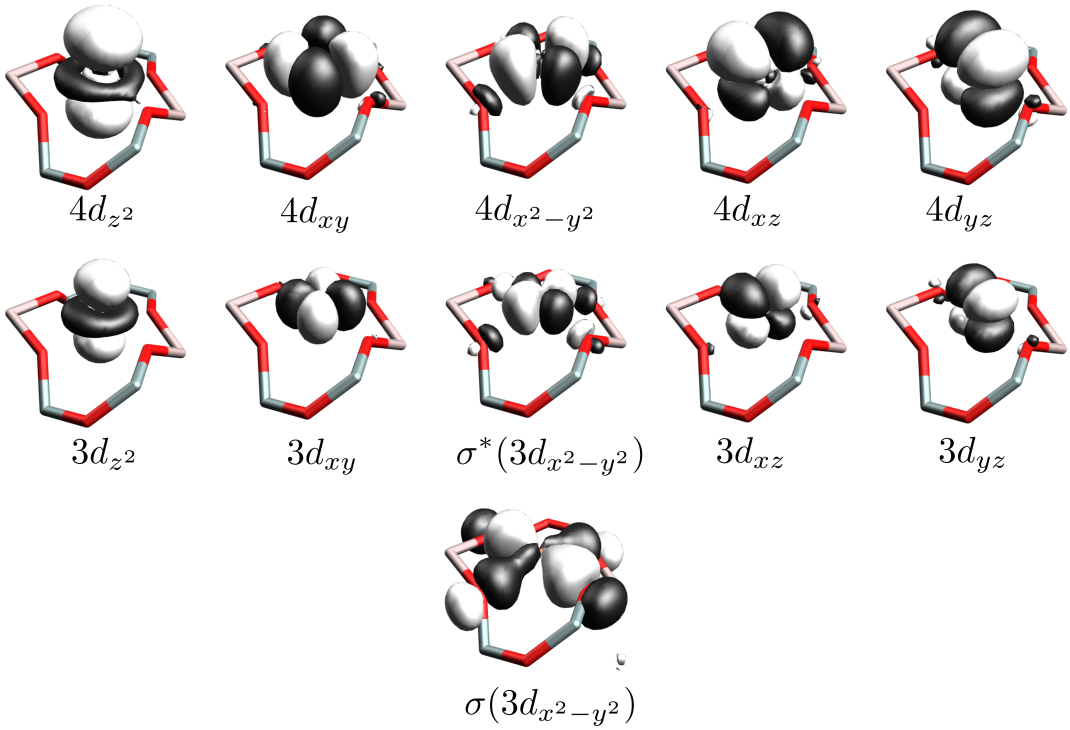

Figure 1: Plot of the active orbitals of the Fe(II)–β(T4T10) cluster in Fe-ZSM-5 (contour values $\pm$0.04 e/a.u.^{3}).

Results and discussion

Location of Fe(II)

The pentasil zeolites ZSM-5 and ferrierite, respectively framework type MFI and FER, exist as single polymorphs. Zeolite Beta, on the other hand, is an intergrowth of two similar polymorphs BEA-A and BEA-B and is denoted as *BEA.[50] A third polymorph (polymorph C) only occurs as a minor impurity in *BEA, but can be synthesized in its pure form and has framework type BEC.[51]

Based on the electronic absorption spectra of bare Co^{2+} in dehydrated Co-zeolites, Wichterlova et al.[52–54] proposed three favorable positions for divalent cations in ZSM-5, zeolite Beta and ferrierite. These are called the α-, β- and γ-site and are shown in Figure 2.

In ZSM-5, the α-site is a planar 6MR along the straight channel. It has an extra O-T-O bridge and can also be seen as two fused 5MRs. The β-site is a planar 6MR at the sinusoidal

channels and has no bridge. The γ-site is a boat shaped 6MR located at the intersection of the straight and the sinusoidal channel with an O-T-O-T-O bridge and can be considered as two fused 6MRs.

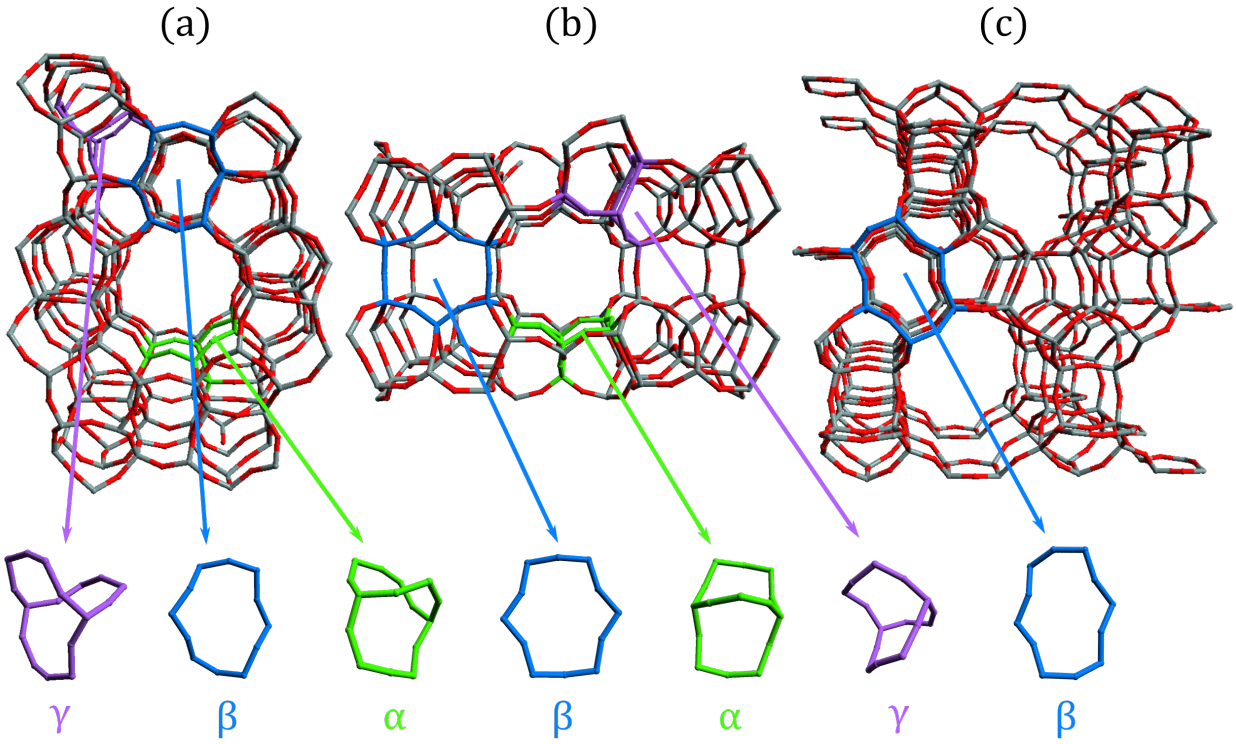

Figure 2: Cation exchange sites containing 6MRs in (a) ZSM-5, (b) FER and (c) BEA morphology A.

In FER, α- and β-sites have similar structures to ZSM-5. The γ-site is also boat shaped but differs form ZSM-5 in that it only has one O-T-O bridge.[54] Only the β-site of this zeolite is modeled in this work. The α-site of ZSM-5 is considered a representative model of all 6MR with one O-T-O bridge, therefore the α- and γ-site in FER are not explicitely considered.

Only Polymorph C of zeolite Beta contains an α-site (6MR with O-T-O bridge).[53] Polymorphs A and B only have a β- and a γ-site. The γ-site in *BEA is completely different from ZSM-5 and FER.[53] As it does not contain a 6MR, we did not consider it in our calculations. The β-rings in polymorphs A and B are similar and a previous study has already shown that there is no significant difference in the calculated spectroscopic properties of Fe(II) in these rings.[21] We therefore only consider the β-ring in polymorph A.

Stability of Fe(II) in the zeolite lattice.

Table 1 summarizes the coordination environment, Fe-O distances, and BEs of Fe(II) at the different cation exchanges sites of the investigated zeolites. Optimized structures are shown in Figure 3. Several sites have a similar coordination environment and in general three coordination types are observed: square pyramidal (Pyr), square planar (SP) and trigonal prismatic (Pris).

Table 1: Summary of coordination numbers, Fe-O distances and BE of the different cluster models at B3LYP level of theory[a].

site	CN[b]	Fe–O (Å)	Fe–O (avg) (Å)	BE
Fe-ZSM-5				
α(T1T7)	Pyr(5)	2.008, 2.168, 2.172, 2.176, 2.118[c]	2.128	597
α(T2T5)	Pyr(5)	2.476, 1.931, 1.998, 1.998, 2.411[c]	2.163	586
α(T2T11)	Pyr(5)	2.212, 2.008, 2.114, 1.941, 2.586[c]	2.172	587
β(T4T10)	SP(4)	1.968, 1.969, 2.060, 2.132	2.032	641
β(T5T11)	SP(4)	1.938, 2.123, 2.010, 2.352[d]	2.106	612
β(T5T10)	SP(4)	1.926, 1.994, 1.961, 2.628[d]	2.127	628
γ(T11T11)	Pris(6)	2.153, 2.130, 2.130,2.153, 2.130, 2.130	2.138	640
γ(T10T11)	Pris(6)	2.381, 2.265, 2.100, 2.138, 2.102, 2.043	2.172	599
γ(T7T12)	SP(4)	1.981, 2.182, 2.341, 2.040[d]	2.136	600
γ(T11T11)$'$	SP(4)	2.048, 2.048, 2.048, 2.058	2.051	628
Fe-BEA				
β(T6T6)	SP(4)	2.021, 2.022, 2.021, 2.022	2.022	631
β(T4T6)	SP(4)	1.972, 2.028, 2.251[d], 1.954	2.051	619
β(T4T4)	SP(4)	1.954, 2.204[d], 1.954, 2.204[d]	2.079	606
Fe-FER				
β(T1T1)	SP(4)	2.020, 2.020, 2.020, 2.020	2.020	647
β(T1T3)	SP(4)	2.338, 1.971, 1.980, 2.159	2.112	635
β(T3T3)	SP(4)	2.299, 2.030, 2.241[d], 1.999	2.143	622

[a] BE are given in kcal/mol and distances in Å
[b] The labels Pyr, SP and Pris are used for distorted square pyramidal, distorted square planar, distorted trigonal prismatic coordination respectively. The coordination number is given between brackets.
[c] Fe$-O_{ax}$, i.e. the distance between Fe and the O at the top of the pyramid.
[d] Fe$-_{Si}O_{Si}$

In a 6MR with a single O-T-O bridge, represented by the α-site in ZSM-5, Fe(II) is coordinated by five framework O in a (distorted) square pyramidal fashion. In the ZSM-5 α-site, the most stable complex is formed at α(T1T7) where Fe(II) is coordinated by

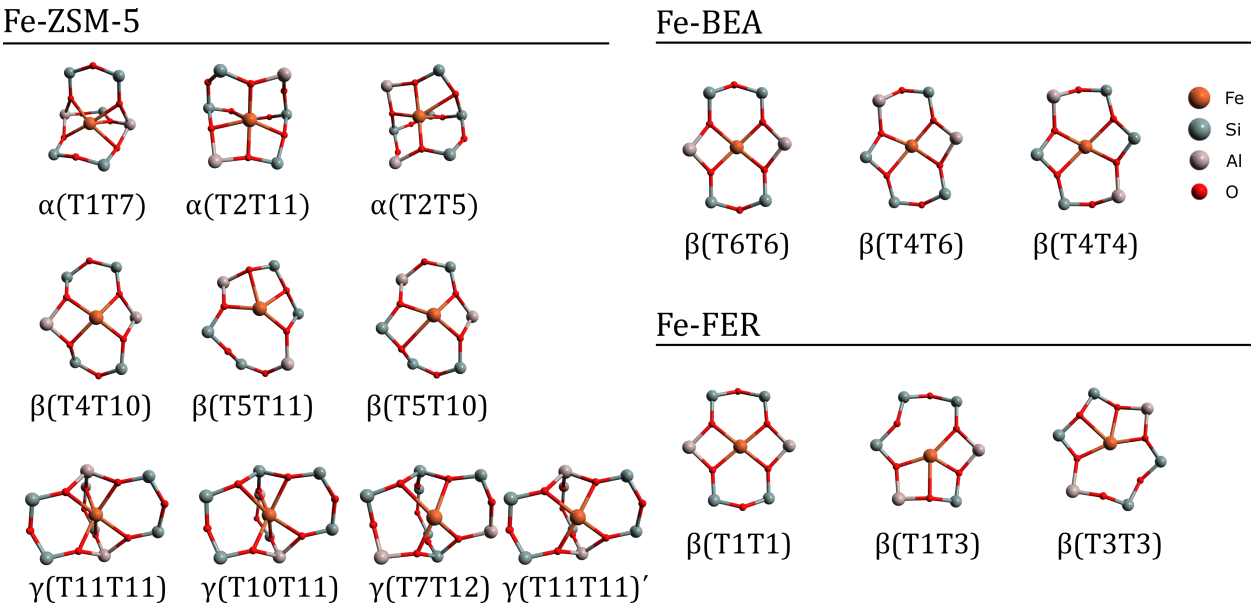

Figure 3: Optimized structures of the cluster models at B3LYP level of theory. End-capping OH are omitted for clarity.

five O atoms that are part of an [AlO_4^-] T-site (O_{Al}). In the other two cases, two of the coordinating O atoms have two neighbouring Si ($_{Si}O_{Si}$). As these are less electron donating than O_{Al}, Fe(II) is less strongly bound at these sites, as shown by the lower BE in Table 1. Obviously, Fe(II) prefers O_{Al} as a ligand and will only accept $_{Si}O_{Si}$ if no O_{Al} is available. This is also reflected by the Fe$-O_{ax}$ distances at the different sites, O_{ax} being the axial oxygen of the square pyramid. In α(T1T7), O_{ax} is an O_{Al}, and the Fe$-O_{ax}$ distance (2.12 Å) is here significantly shorter than in the two other clusters α(T2T5) (2.41 Å) and α(T2T11) (2.57 Å), where O_{ax} is an $_{Si}O_{Si}$.

At the β-site in ZSM-5 (and the other two zeolites, see further), Fe(II) is coordinated in a (distorted) square planar fashion. Similar to the α-site, the most stable complex is formed when Fe(II) is only coordinated by O_{Al}, that is at β(T4T10). This site has the highest of all BEs and is thus expected to be most favorable for Fe(II) coordination. At the other two β sites one Fe$-_{Si}O_{Si}$ bond occurs, which is significantly longer than the other three Fe$-O_{Al}$ bonds, explaining the lower BE of these two models. Despite the longer Fe$-_{Si}O_{Si}$ in β(T5T10), we find that Fe(II) is more strongly bound in this ring than in β(T5T11). As can

be seen from Figure 3 the coordination environment is in β(T5T11) considerably distorted from regular square planar, explaining its lower BE.

At the γ-site in ZSM-5, both a six-fold Pris(6) (distorted trigonal prism) and a four-fold SP(4) (distorted square planar) Fe(II) coordination can be obtained as a minimum on the potential energy surface. The four coordinated structure is the most stable for γ(T7T12), whereas a six coordinated structure is found more stable for γ(T11T11) and γ(T10T11). Again, Fe(II) binds most strongly when it can coordinate with a maximum number of O_{Al}, six in this case at γ(T11T11).

In general, our results for Fe-ZSM-5 are in good agreement with a previous periodic DFT study.[13] At the α- and β-sites Li et al.[13] also calculated a square pyramidal and square planar coordination respectively. However, at the γ-site (called δ in ref 13) only four-fold coorination was reported for all Al distributions, whereas we find a six-fold Pris(6) coordination to be more stable at γ(T11T11) and γ(T10T11). This difference may be caused by the use of a different functional in the geometry optimizations: PBE in the periodic DFT calculations versus B3LYP in our cluster models. This was further investigated by comparing the stability of the four-fold relative to six-fold coordination at the DFT (B3LYP and PBE functional) and CASPT2 levels of theory (shown in Table 2). For γ(T7T12) the three methods predict the four-fold coordination to be the most stable, in accordance with ref. 13. At γ(T10T11), the six-fold coordination is for all methods the most stable (this site was not considered in ref. 13). However, for γ(T11T11) the results are method dependent. With B3LYP, the four-fold coordinated structure is almost 12 kcal/mol higher in energy than the six-fold coordinated structure. On the other hand, with PBE (the functional of ref. 13) it is 4 kcal/mol lower in energy. Single point CASPT2 calculations at the DFT B3LYP structures predict that both geometries are very close in energy ($\approx$1 kcal/mol). Thus, whether the four-fold coordinated or the six-fold coordinated species is the most stable is rather dependent on the applied functional than on the model (cluster model versus periodic DFT study) and no conclusive answer on the coordination of Fe(II) at γ(T11T11) can be given from these calculations.

Therefore, both structures are used in the calculation of the d-d transitions. The four-fold coordinated structure is denoted as γ(T11T11)$'$.

As the binding energies in Table 1 were obtained using cluster models differing in size, comparing these data between different sites in Fe-ZSM-5 must be done with great caution. Previous results for the BEs obtained from the periodic DFT-PBE study of Li et al.[13] should be considered more trustworthy. In that study, the most stable configuration is the one with Fe(II) located at γ(T11T11)$'$, followed by β(T4T10) at 8.6 kcal/mol, and α(T1T7) at 15.3 kcal/mol. Here, we find that binding at β(T4T10) is slightly more favorable than at γ(T11T11). Importantly, however, both studies agree that Fe(II) binding is energetically least favorable at the α-sites, although the difference in binding energy between the α-sites and the other two sites (40 kcal/mol) is probably grossly overestimated by the cluster model calculations presented in Table 1.

Table 2: Stability of the four-coordinated structures relative to the six-coordinated structures of Fe(II) at different γ-rings in ZSM-5 (in kcal/mol).

Level of theory	γ(T11T11)	γ(T10T11)	γ(T7T12)
DFT-B3LYP	12.0	12.2	-10.1
DFT-PBE	-4.2	13.5	-15.8
CASPT2	-1.4	15.2	-10.1

As in ZSM-5, Fe(II) also has a distorted square planar SP(4) coordination at the β-site in FER. The highest BE is obtained for β(T1T1) where Fe(II) has the opportunity to bind to four O_{Al}, similar to the β(T4T10) site in Fe-ZSM-5. In β(T1T3) Fe(II) is also coordinated to four O_{Al}, but to reach this coordination it has to move away from the center of the ring towards the two Al, giving rise to a strongly distorted SP(4) structure with one longer Fe–O bond (2.33 Å). This less favorable situation gives rise to a smaller BE. β(T3T3) also has a very distorted SP(4) structure but here Fe(II) is bound to one $_{Si}O_{Si}$, giving the least stable Fe coordination.

At the β-site in *BEA, Fe(II) is always coordinated by the four O closest to the center of the ring. Also here the most stable complex is obtained when Fe(II) is bound to four O_{Al},

that is in β(T6T6). The BE in the other two rings decreases with the number of coordinating O_{Al}.

In summary, our results point to a crucial role of the Al-distribution in zeolites for strong Fe(II) coordination. Obviously, the Fe(II) ion shows a strong propensity to form a maximum number of Fe$-O_{Al}$ bonds. The most stable configuration is systematically obtained when the two framework Al ions are positioned in a symmetric fashion in the 6MR, opposite but at the closest possible distance to each other. This way, four short Fe$-O_{Al}$ bonds can be formed in the 6MR in a close to perfect square planar configuration, as is the case for β(T1T1) in FER, β(T6T6) in *BEA, β(T4T10) and γ(T11T11)$'$ in ZSM-5. Possibly, two extra Fe$-O_{Al}$ bonds may be formed at the latter site to form a Pris(6) in γ(T11T11). The five-coordinated Pyr(5) configuration at the α(T1T7) site in ZSM-5 has five Fe$-O_{Al}$ bonds, but this configuration is significantly less stable, as was already noted before by Li et al.[13] With the framework Al at less favorable positions, Fe$-O_{Al}$ bonds can only be formed at the expense of substantial deformation of the 6MRs, giving rise to distorted SP(4) configurations or to situations where Fe has to settle for Fe$-_{Si}O_{Si}$ bonds instead. These are all factors that diminish the average strength of the Fe–O interactions, making it less likely that Fe(II) will bind at these sites.

Ligand field spectra

Different Fe(II) coordination environments at the different cation exchange sites should also give rise to different splittings of the metal 3d orbitals. A qualitative orbital splitting scheme for each of the coordination types described above is provided in Figure 4. The levels drawn next to each other would be degenerated in a strictly symmetric environment, but are split because of geometrical distortions. In high-spin Fe(II) complexes, four spin allowed excitations within the d shell can occur, each exciting an electron from the doubly occupied orbital in the ground state into one of the other four d-orbitals. The calculated transition energies are given in Table 3. The experimental DR-UV-vis spectra of the three Fe-zeolites were reported previously[21] and are reproduced in Figure 5. In the 5 000–25 000 cm^{-1}

region, all three spectra show their most intense LF band at around 16 000 cm^{-1}. This is the band that correlates with α-Fe, as it disappears upon activation by N_2O to form α-oxygen. Other, weaker features appear in the 5 000–10 000 cm^{-1} region, with a band at around 10 000 cm^{-1} most prominently present in Fe-ZSM-5, and appearing as a shoulder in the other two zeolites. All features in this region should be attributed to 'spectator' Fe(II),[21] as they remain unaffected in the N_2O- and CH_4-reacted spectrum (see Figure 5a). The intensity of these bands increases with increasing Fe loading (as shown in Figure 5b for Fe-ZSM-5), whereas the α-Fe band is already saturated at low iron loadings, indicating that the former sites are less stable than α-Fe.

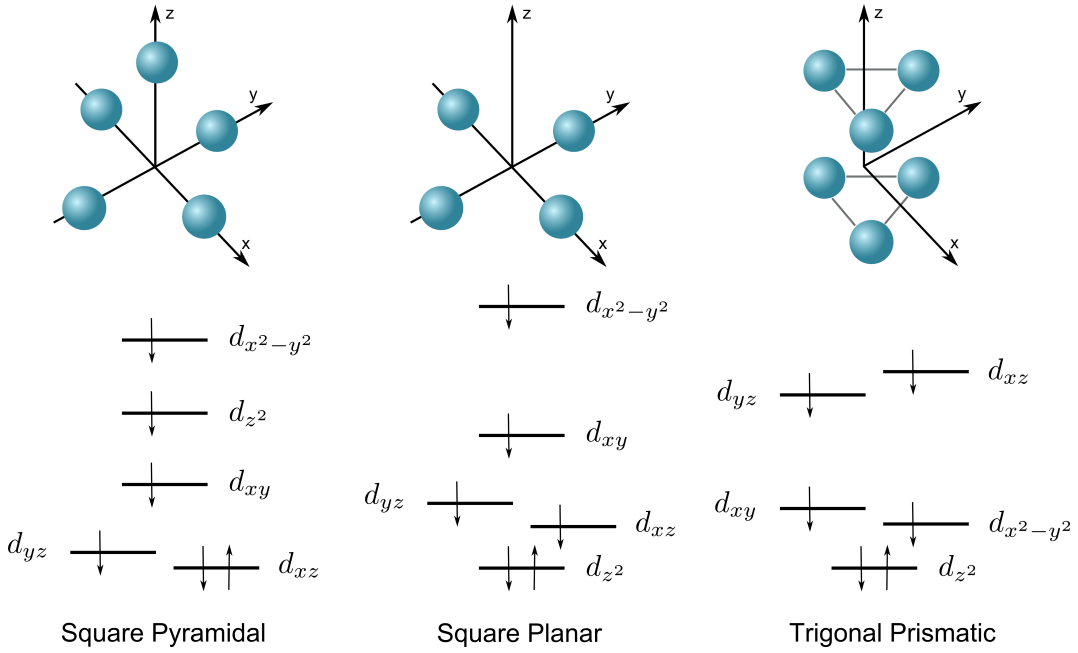

Figure 4: Splitting of the 3d orbitals for different Fe(II) coordination environments in Fe-ZSM-5.

In a square planar configuration only one of the Fe 3d orbitals, $3d_{x^2-y^2}$, is involved in a covalent σ interaction with the surrounding O, and is strongly destabilized (Figure 1). The other four orbitals essentially remain pure 3d, but are of course also destabilized by electrostatic interaction with the 'hard' oxygen environment, of π- (d_{xy}, d_{xz}, d_{yz}) or σ-type (d_{z^2}). The latter orbital has the lowest energy and is doubly occupied in the ground state. As we will show in the next section, this is partly related to the stabilizing effect of 3d-4s

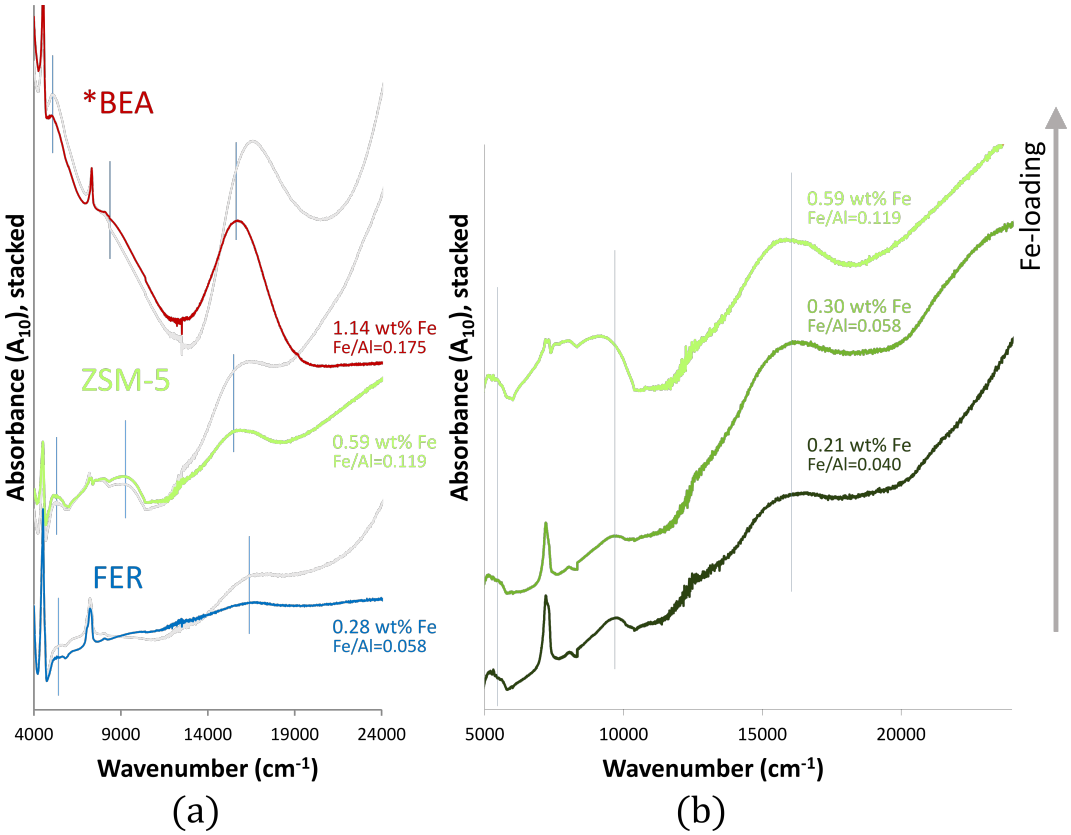

Figure 5: DR-UV-Vis spectra of (a) Fe(II)-*BEA, Fe(II)-ZSM-5, and Fe(II)-FER (grey curve shows the spectrum of the same sample after N_2O treatment) (b) Fe(II)-ZSM-5 with different Fe-loadings. Reproduced from ref 21.

mixing on the $3d_{z^2}$ orbital. In all models with a SP(4) configuration the highest LF transition therefore corresponds to a $d_{z^2} \rightarrow d_{x^2-y^2}$ excitation. Naturally, the highest excitation energies, 15 000–17 000 cm^{-1}, are calculated for 6MRs with the most regular square planar configuration, giving the strongest $d_{x^2-y^2}$–O σ interaction, that is in β(T4T10) and γ(T11T11)′ of Fe-ZSM5, β(T6T6) of Fe-*BEA and β(T1T1) of Fe-FER. The calculated transition energies for the β sites nicely follow the ordering of the experimental band positions of the α-Fe band in the respective zeolites: 15 005 cm^{-1} for β(T4T10) in Fe-ZSM-5 (α-Fe band 15 200 cm^{-1}) < 16 053 cm^{-1} for β(T6T6) in Fe-Beta (α-Fe band 15 900 cm^{-1}) < 17 364 cm^{-1} for β(T1T1) in Fe-FER (α-Fe band 16 100 cm^{-1}). The deviation from experiment is largest in the latter case, but still lies within the 'normal' error bars of the CASPT2 method (2 500 cm^{-1}). All other SP(4) configurations give rise to a weaker oxygen ligand field, with $d_{z^2} \rightarrow d_{x^2-y^2}$ exci-

tation energies between 14 300 cm^{-1} and as low as 9 400 cm^{-1}. As shown above, these are the sites where Fe can only bind to four O_{Al} at the expense of strong distortions or where it has to settle for an Fe$-_{Si}O_{Si}$ instead of an Fe$-O_{Al}$ bond. Both situations gives rise to a weakening of the $d_{x^2-y^2}$–O interaction, thus leading to a red shift of the $d_{z^2}\rightarrow d_{x^2-y^2}$ transition. Therefore, these results confirm the conclusions drawn from the calculated BEs in the previous section, that Fe(II) prefers to be located at β-sites that can provide a 'symmetric' Al distribution in the 6MR.

In a square pyramidal configuration, the d_{z^2} orbital is destabilized by σ interaction with the axial oxygen and the highest LF excitation now corresponds to $d_{yz}\rightarrow d_{x^2-y^2}$. The calculated transition energy, 12 000–13 000 cm^{-1}, is considerably lower than for the 'ideal' SP(4) complexes, and does not correspond to a band in the experimental spectrum. Together with the BE arguments, this strengthens our conclusion that Fe(II) prefers not to bind at 6MRs with a bridging O-T-O in any but low concentrations, assuming that such sites exist in the investigated zeolites.

In a perfect trigonal prism (D_{3h}) the 3d orbitals are split into $a_1^{'}(d_{z^2})$, $e^{'}(d_{xz},d_{yz})$, $e^{''}(d_{x^2-y^2},d_{xy})$, where $a_1^{'}(d_{z^2})$ is least destabilized by the ligand field. As both the $e^{'}$ and $e^{''}$ shells involve a mixture of σ and π interactions with the surrounding O, the ligand field splitting should be significantly smaller in the Pris(6) clusters than the $d_{xy}\rightarrow d_{x^2-y^2}$ transition in the symmetric SP(4) clusters. Indeed, the highest excitation energy obtained from the CASPT2 calculations for the trigonal prismatic γ sites in Fe-ZSM-5 amounts to only 10 700 cm^{-1} (transition $d_{z^2}\rightarrow d_{xz}$). The experimental spectrum of Fe-ZSM-5 shows a distinct 'spectator' LF band at around 10 000 cm^{-1}. As these sites also show a high stability (even the highest in the periodic DFT) it is highly likely that the 10 000 cm^{-1} band in Fe-ZSM-5 is caused by six-coordinate Fe coordinated at 6MR with a bridging O-T-O-T-O. Similar structures should be held responsible for the (weaker) 10 000 cm^{-1} feature in the other two zeolites. The lack of reactivity of these spectator sites should be attributed to their saturated six-fold coordination, leaving no room for an attacking N_2O.

Table 3: Calculated excitation energies of the different clusters at CASPT2[a] level of theory (in cm^{-1}) and experimental band position of the α-Fe band.

Fe-ZSM-5 (exp.[b] : 15 200 cm^{-1})					
Square pyramidal	α(T1T7)	α(T2T5)	α(T2T11)		
$d_{yz}\rightarrow d_{xz}$	1 876	3 137	1 648		
$d_{yz}\rightarrow d_{xy}$	3 864	3 099	3 863		
$d_{yz}\rightarrow d_{z^2}$	7 225	4 904	5 020		
$d_{yz}\rightarrow d_{x^2-y^2}$	11 933	12 938	13 020		
Square planar	β(T4T10)	β(T5T11)	β(T5T10)	γ(T11T11)$'$	γ(T7T12)
$d_{z^2}\rightarrow d_{yz}$	1 904	672	1 153	2 069	1 789
$d_{z^2}\rightarrow d_{xz}$	2 428	3 583	3 105	2 166	2 400
$d_{z^2}\rightarrow d_{xy}$	3 613	7 312	4 789	3 881	3 900
$d_{z^2}\rightarrow d_{x^2-y^2}$	15 005	9 402	11 456	14 996	12 610
Trigonal prismatic	γ(T11T11)	γ(T10T11)			
$d_{z^2}\rightarrow d_{xy}$	5 867	4 443			
$d_{z^2}\rightarrow d_{x^2-y^2}$	6 273	4 922			
$d_{z^2}\rightarrow d_{yz}$	9 854	8 355			
$d_{z^2}\rightarrow d_{xz}$	10 677	10 707			
Fe-Beta (exp.[b] : 15 900 cm^{-1})					
Square planar	β(T6T6)[b]	β(T4T6)[b]	β(T4T4)[b]		
$d_{z^2}\rightarrow d_{yz}$	2 179	1 590	473		
$d_{z^2}\rightarrow d_{xz}$	3 024	3 066	3 812		
$d_{z^2}\rightarrow d_{xy}$	4 027	4 632	4 426		
$d_{z^2}\rightarrow d_{x^2-y^2}$	16 053	14 361	13 114		
Fe-FER (exp.[b] : 16 100 cm^{-1})					
Square planar	β(T1T1)	β(T1T3)	β(T3T3)		
$d_{z^2}\rightarrow d_{yz}$	1 881	1 084	576		
$d_{z^2}\rightarrow d_{xz}$	2 396	2 913	3 135		
$d_{z^2}\rightarrow d_{xy}$	4 411	7 949	6 966		
$d_{z^2}\rightarrow d_{x^2-y^2}$	17 364	10 504	9 354		

[a] CASPT2 calculations are performed on a CAS(8,11) reference function in the case of the square planar and square pyramidal structures and a CAS(10,12) reference in the case of the trigonal prismatic structures.
[b] Experimental values taken from ref 21

Finally, the question remains whether β(T4T10) is the exclusive α-Fe site inFe-ZSM-5 , or whether a four-fold coordinated Fe(II) at γ(T11T11)$'$ might also show distinct reactivity towards N_2O. No conclusive answer can be formulated based on our calculations. However, in this respect the experimental work of Sazama et al.[8] is informative; Different ZSM-5

zeolites were synthesized containing the same Si/Al ratio, but with different distributions of Al in the framework. It was concluded that a larger amount of Al-O-Si-O-Si-O-Al sequences (denoted as Al-pairs) in 6MRs stabilize the formation of Fe(II) in Fe-ZSM-5. The largest amounts of such Al pairs were located within the β-ring (approx. 60%) whereas the γ-ring contained the lowest amount of Al pairs (less then 10%).[8] Based on these results, one might expect the α-Fe species to be located primarily at the β(T4T10) position, and to be the main responsible for the band at 15 200 cm^{-1} in the experimental LF spectrum.

Stability of square planar Fe(II)

In a square planar complex, the ligand lone pairs are pointed directly towards the metal $d_{x^2-y^2}$ orbital. In a field of four strong σ-donors this leads to a substantial destabilization of this orbital, which therefore normally remains unoccupied, the remaining four 3d orbitals being filled according to Hund's rule. In d^6 systems, this should result in a triplet spin state (S=1).[55] Thus, square planar Fe(II) complexes almost invariably have a triplet ground state, as found in four-coordinated ferrous porphyrins.[56] If the field of the ligands is weak(er), four-coordinated Fe(II) complexes can be high spin (S=2). However, then a tetrahedral geometry is expected because this reduces the antibonding character of the $d_{x^2-y^2}$ orbital.[55]

For this reason, it has long been accepted that the experimentally observed square planar structure of high-spin Fe(II)O_4 in different solid state environments is in fact enforced by geometric constraints imposed by the environment.[24–26] Doubts about this were raised when the first molecular (S=2) complexes with a square planar FeO_4 configuration were presented in the literature,[23,27] suggesting that a square planar coordination environment might in fact be electronically preferred by high-spin Fe(II) in specific ligand environments. Based on our observations in the previous sections, that the most stable configurations are systematically obtained when Fe(II) can bind at 6MRs with an oxygen configuration that is *least* distorted from square planar, it is more than likely that such a square planar oxygen coordination environment is indeed preferred rather than imposed in a zeolite environment. In order

to assess the stability of SP Fe(II) compared to its tetrahedral counterpart, we decided to investigate the geometric and electronic structure of a cluster model that mimics the α-Fe site as realistically as possible but excluding any possible strain. Starting from one of the β-type 6MRs with the appropriate Al distribution (e.g. the β(T4T10) cluster of Fe-ZSM-5) the two Si–O–Si bridges were removed and the four Si were replaced by H, thus resulting in FeL_2 with $L = [Al(OH)_4]^-$. A series of geometry optimizations were performed on this cluster model with DFT (B3LYP), fixing the dihedral angle between the planes formed by the two FeO_2 triangles at values ranging between $\delta = 0°$ (square planar) to $\delta = 90°$(tetrahedral). Single point CASPT2 calculations were also performed for each of the structures. The resulting potential energy scans are shown in Figure 6. With B3LYP the curve has its minimum energy structure in between square planar and tetrahedral ($\delta \approx 45°$), while it is shifted more towards square planar with CASPT2 ($\delta \approx 35°$). Importantly, both levels of theory predict very flat curves, with a maximum energy barrier of 2.5 kcal/mol (B3LYP) to reach the tetrahedron, while less than 1 kcal/mol with B3LYP and only 0.5 kcal/mol with CASPT2 is needed to flatten the structure to an 'ideal' square plane. The maximum geometric strain that could be exerted by the zeolite on the α-Fe site in the three zeolites is therefore estimated to be 1 kcal/mol.

The transformation path shown in Figure 6 closely corresponds to a similar curve for the simpler $[Fe(OH)_4]^{2-}$ model presented by Wurzenberger et al.[27], which was also found to be very flat with the square plane more stable than the tetrahedron and the minimum lying in between. The flattening of the tetrahedron was rationalized as a Jahn Teller (JT) effect, occurring for ligand donor atoms that, apart from a weak-field character (ensuring the high spin case) should have the following properties: (a) strong enough π-basicity to raise the d_{xy}, d_{yz}, d_{xz} orbitals above d_{z^2} such that the latter orbital is doubly occupied in the ground state, (b) a high non-delocalized negative charge, creating a strong repulsive force with the main lobe of the doubly occupied d_{z^2} orbital which can be reduced upon flattening, although it has to overcome the counteracting increase in interligand repulsion. Both conditions are fulfilled

in the present zeolite case. As seen in the previous section, the ground state in the SP(4) complexes has d_{z^2} doubly occupied, while the pure d character of the d_{xy}, d_{yz}, d_{xz} orbitals in Figure 1 is indicative of a hard Fe–O π-interaction with no delocalization of oxygen charge in the metal d shell. However, a third factor, which has not been discussed before, might come into play that can provide extra stabilization to the square planar structure and has not been discussed before, that is mixing of the $3d_{z^2}$ orbital with the higher-lying 4s orbital. Such mixing is symmetry forbidden in the tetrahedron but becomes allowed when the structure is flattened to a square plane, where it serves (a) to further stabilize the $3d_{z^2}$ orbital, and (b) to increase the probability density of its axial lobe (at the expense of its toroidal ring). Both factors are expected to strengthen the driving force behind the JT flattening of the FeO_4 configuration.

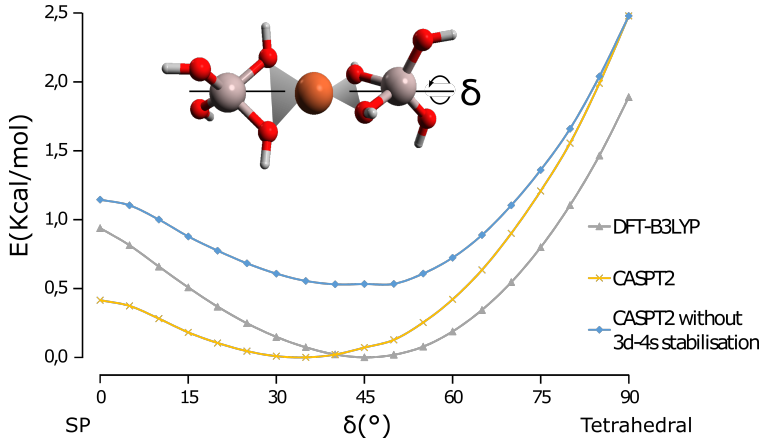

Figure 6: Potential energy of $Fe[Al(OH)_4]_2$ as a function of the dihedral angle δ between two FeO_2 triangles, obtained from B3LYP and CASPT2.

Inspection of the (Mulliken) composition of the $3d_{z^2}$ natural orbital in the different α-Fe model clusters (β(T4T10), and γ(T11T11)' in Fe-ZSM-5, β(T6T6) in Fe-BEA, β(T1T1) in Fe-FER) shows that the contribution of 4s is small but significant: 2.1–3.3%. In order to quantify the effect of $3d_{z^2}$-4s mixing on the shape of the CASPT2 curve in Figure 6, the following procedure was used. First, an extra CASSCF calculation was performed for each δ, where the ANO basis set on Fe was reduced to [**3s**6p5d3f2g1h] (rather than the original [**7s**6p5d3f2g1h]). As the new basis set lacks the 4s orbital it cannot describe $3d_{z^2}$-4s mixing,

therefore the energy difference between the CASSCF energy obtained with the two basis sets, $\Delta E_{\mathrm{CAS}}(\delta)$, contains the $3d_{z^2}$-4s stabilization energy $\Delta E_{d-s}(\delta)$, next to the mere effect of the extra diffuse s functions in the original basis set on the CASSCF energy. The latter was corrected for by reducing each $\Delta E_{\mathrm{CAS}}(\delta)$ with its value at $\delta = 90°$, i.e. the tetrahedral structure where $3d_{z^2}$-4s mixing is absent.

$$\Delta E_{d-s}(\delta) = \Delta E_{\mathrm{CAS}}(\delta) - \Delta E_{\mathrm{CAS}}(\delta = 90°) \tag{2}$$

The blue curve in Figure 6 is obtained by substracting $\Delta E_{d-s}(\delta)$ from the CASPT2 energy at each δ. As expected, the effect of $3d_{z^2}$-4s indeed steadily grows as the structure is flattened, reaching a maximum of 0.7 kcal/mol at $\delta = 0°$. This is more than one third of the total CASPT2 energy difference between the square planar and tetrahedral structure, making $3d_{z^2}$-4s mixing an important stabilising factor of high-spin square planar Fe(II) complexes. Excluding $3d_{z^2}$-4s mixing, the CASPT2 minimum lies significantly closer to the tetrahedral structure ($\delta = 45°$) and the energy required to reach the ideal square plane is slightly increased to 0.7 kcal/mol. We note that $3d_{z^2}$-4s mixing has been invoked previously to explain the extra stabilization of the d_{z^2} orbital in square planar complexes of late transitions metals[57] (Cu(II),[58] Ni(II),[59] Pt(II) and Pd(II)[60]). To the best of our knowledge, we are the first to report such an effect in square planar Fe(II) complexes.

Conclusion

Making use of DFT and CASPT2 computations on a series of cluster models representing the 6MRs in the zeolites ZSM-5, BEA and FER, combined with previously obtained experimental spectroscopic data[21] we can unequivocally assign α-Fe in all three zeolites as a high-spin square planar Fe(II) bound to β-type 6MRs containing the sequence Al-Si-Si-Al, with the Al positioned opposite in the ring and as close as possible to each other. This way, a regular square planar FeO_4 configuration with four short Fe-O bonds can be formed. The

α-Fe band in the LF spectra of the three zeolites was accurately reproduced by CASPT2 calculations (only) for these specific β-type cluster models, and was assigned as a $d_{z^2} \rightarrow d_{x^2-y^2}$ transition. Spectator band(s) at lower wavelengths most probably originate from high-spin Fe(II) in a six-coordinated trigonal prismatic oxygen environment, that can be obtained in 6MRs with an additional O-T-O-T-O bridge, such as the γ-sites in ZSM-5. On the other hand, 6MRs with an O-T-O bridge such as the α-sites in ZSM-5, where Fe(II) could adopt a five-coordinated square pyramidal configuration, are not likely to bind Fe(II).

The calculations indicate that the square planar coordination environment, although uncommon for high-spin Fe(II), is not imposed by the zeolite lattice, but rather is electronically preferred by Fe(II) in the specific environment offered by the lattice oxygens. The crucial factor for this electronic preference is the double occupancy of the $3d_{z^2}$ orbital in the ground state. Electronic repulsion between the axial lobe of $3d_{z^2}$ and the hard, negatively charged oxygens, is the driving force for a flattening of the FeO_4 configuration from the 'expected' tetrahedron towards square planar. We have also demonstrated that mixing of $3d_{z^2}$ with the higher-lying 4s orbital significantly contributes to this driving force.

That the zeolite lattice does not force the metal into a strained geometry does not mean that it does not play an 'entatic' role in the catalytic methane to methanol transformation. On the contrary, by providing the Fe(II) ion with a stable weak-field square planar oxygen coordination, where coordination of extra lattice oxygens is energetically unfavorable, the zeolite opens the way for efficient oxygen transfer from N_2O to form the active α-O intermediate, a high-spin square pyramidal ^{5}Fe(IV)=O species. As was shown previously, geometric strain from the zeolite lattice does aid in activating this species for reaction with CH_4.[21]

Acknowledgement

This investigation has been supported by the Flemish Science Foundation (FWO, grants G0A2216N to B.F.S and G.0865.13 to K.P.). S.D.H. acknowledges FWO for a PhD (aspirant)

Fellowship. The computational resources and services used in this work were provided by the VSC (Flemish Supercomputer Center), funded by the Hercules Foundation and the Flemish Government - department EWI. The COST Action ECOSTBio CM1305 from the European Union is also gratefully acknowledged.

Supporting Information Available

The atomic coordinates of all the optimised structures. This material is available free of charge via the Internet at http://pubs.acs.org/.

References

(1) De Montellano, P. R. O. *Cytochrome P450: structure, mechanism, and biochemistry*; Springer Science & Business Media, 2005.

(2) Shaik, S.; Kumar, D.; de Visser, S. P.; Altun, A.; Thiel, W. Theoretical perspective on the structure and mechanism of cytochrome P450 enzymes. *Chem. rev.* **2005**, *105*, 2279–2328.

(3) Merkx, M.; Kopp, D. A.; Sazinsky, M. H.; Blazyk, J. L.; Müller, J.; Lippard, S. J. Dioxygen Activation and Methane Hydroxylation by Soluble Methane Monooxygenase: A Tale of Two Irons and Three Proteins. *Angew. Chem. Int. Ed.* **2001**, *40*, 2782–2807.

(4) McDonald, A. R.; Que, L. High-valent nonheme iron-oxo complexes: Synthesis, structure, and spectroscopy. *Coord. Chem. Rev.* **2013**, *257*, 414–428.

(5) Sobolev, V.; Dubkov, K.; Panna, O.; Panov, G. Selective oxidation of methane to methanol on a FeZSM-5 surface. *Catal. today* **1995**, *24*, 251–252.

(6) Panov, G.; Sheveleva, G.; Kharitonov, A. e. a.; Romannikov, V.; Vostrikova, L. Oxi-

dation of benzene to phenol by nitrous oxide over Fe-ZSM-5 zeolites. *Appl. Catal., A* **1992**, *82*, 31–36.

(7) Dubkov, K.; Sobolev, V.; Talsi, E.; Rodkin, M.; Watkins, N.; Shteinman, A.; Panov, G. Kinetic isotope effects and mechanism of biomimetic oxidation of methane and benzene on FeZSM-5 zeolite. *J. Mol. Catal. A* **1997**, *123*, 155–161.

(8) Sazama, P.; Wichterlová, B.; Tábor, E.; Štástnỳ, P.; Sathu, N. K.; Sobalík, Z.; Dědeček, J.; Sklenák, Š.; Klein, P.; Vondrová, A. Tailoring of the structure of Fe-cationic species in Fe-ZSM-5 by distribution of Al atoms in the framework for N_2O decomposition and $NH_3-SCR-NO_x$. *J. Catal* **2014**, *312*, 123–138.

(9) Jia, J.; Wen, B.; Sachtler, W. M. Identification by Isotopic Exchange of Oxygen Deposited on Fe/MFI by Decomposing N_2O. *J. Catal* **2002**, *210*, 453–459.

(10) Guesmi, H.; Berthomieu, D.; Kiwi-Minsker, L. Reactivity of oxygen species formed upon N_2O dissociation over Fe–ZSM-5 zeolite: CO oxidation as a model. *Catal. Commun.* **2010**, *11*, 1026–1031.

(11) Roy, P. K.; Pirngruber, G. D. The surface chemistry of N_2O decomposition on iron-containing zeolites (II)The effect of high-temperature pretreatments. *J. Catal* **2004**, *227*, 164–174.

(12) Pirngruber, G. D.; Roy, P. K.; Prins, R. On determining the nuclearity of iron sites in Fe-ZSM-5: a critical evaluation. *Phys. Chem. Chem. Phys.* **2006**, *8*, 3939–3950.

(13) Li, G.; Pidko, E. A.; van Santen, R. A.; Feng, Z.; Li, C.; Hensen, E. J. Stability and reactivity of active sites for direct benzene oxidation to phenol in Fe/ZSM-5: a comprehensive periodic DFT study. *J. Catal* **2011**, *284*, 194–206.

(14) Yoshizawa, K.; Shiota, Y.; Yumura, T.; Yamabe, T. Direct methane-methanol and

benzene-phenol conversions on Fe-ZSM-5 zeolite: Theoretical predictions on the reaction pathways and energetics. *J. Phys. Chem. B* **2000**, *104*, 734–740.

(15) Kachurovskaya, N. A.; Zhidomirov, G. M.; Hensen, E. J.; van Santen, R. A. Cluster model DFT study of the intermediates of benzene to phenol oxidation by N2O on FeZSM-5 zeolites. *Cat. Let.* **2003**, *86*, 25–31.

(16) Fellah, M. F.; Pidko, E. A.; van Santen, R. A.; Onal, I. A DFT study of direct oxidation of benzene to phenol by N2O over [Fe (μ-O) Fe] 2+ complexes in ZSM-5 zeolite. *J. Phys. Chem. C* **2011**, *115*, 9668–9680.

(17) Ryder, J. A.; Chakraborty, A. K.; Bell, A. T. Density functional theory study of benzene oxidation over Fe-ZSM-5. *J. Catal* **2003**, *220*, 84–91.

(18) Goltl, F.; Michel, C.; Andrikopoulos, P. C.; Love, A. M.; Hafner, J.; Hermans, I.; Sautet, P. Computationally Exploring Confinement Effects in the Methane-to-Methanol Conversion Over Iron-Oxo Centers in Zeolites. *ACS Catal.* **2016**, *6*, 8404–8409.

(19) Zecchina, A.; Rivallan, M.; Berlier, G.; Lamberti, C.; Ricchiardi, G. Structure and nuclearity of active sites in Fe-zeolites: comparison with iron sites in enzymes and homogeneous catalysts. *Phys. Chem. Chem. Phys.* **2007**, *9*, 3483–3499.

(20) Smeets, P. J.; Woertink, J. S.; Sels, B. F.; Solomon, E. I.; Schoonheydt, R. A. Transition-metal ions in zeolites: coordination and activation of oxygen. *Inorg. Chem.* **2010**, *49*, 3573–3583.

(21) Snyder, B. E.; Vanelderen, P.; Bols, M. L.; Hallaert, S. D.; Böttger, L. H.; Ungur, L.; Pierloot, K.; Schoonheydt, R. A.; Sels, B. F.; Solomon, E. I. The active site of low-temperature methane hydroxylation in iron-containing zeolites. *Nature* **2016**, *536*, 317–321.

(22) Vallee, B. L.; Williams, R. Metalloenzymes: the entatic nature of their active sites. *Proc. Natl. Acad. Sci.* **1968**, *59*, 498–505.

(23) Holland, P. L. Coordination chemistry: All square for high-spin iron(II). *Nat. Chem.* **2011**, *3*, 507–508.

(24) Burns, R. G.; Clark, M. G.; Stone, A. J. *Inorg. Chem.* **1966**, *5*, 1268–1272.

(25) Tujimoto, Y.; Tassel, C.; Hayashi, N.; Watanabe, T.; Kageyama, H.; Yoshimura, K.; Takano, M.; Ceretti, M.; Ritter, C.; Paulus, W. Infinite-layer iron oxide with a square-planar coordination. *Nature* **2007**, *450*, 1062–1066.

(26) Tassel, C.; Pruneda, J. M.; Hayashi, N.; Watanabe, T.; Kitada, A.; Tsujimoto, Y.; Kageyama, H.; Yoshimura, K.; Takano, M.; Nishi, M.; Ohoyama, K.; Mizumaki, M.; Naomi, K.; Íñiguez, J.; Canadell, E. $CaFeO_2$: a new type of layered structure with iron in a distorted square planar coordination. *J. Am. Chem. Soc.* **2009**, *131*, 221–229.

(27) Wurzenberger, X.; Piotrowski, H.; Klüfers, P. A Stable Molecular Entity Derived from Rare Iron (II) Minerals: The Square-Planar High-Spin-d6 FeIIO4 Chromophore. *Angew. Chem. Int. Ed.* **2011**, *50*, 4974–4978.

(28) Cantalupo, S. A.; Fiedler, S. R.; Shores, M. P.; Rheingold, A. L.; Doerrer, L. H. High-Spin Square-Planar CoII and FeII Complexes and Reasons for Their Electronic Structure. *Angew. Chem. Int. Ed.* **2012**, *51*, 1000–1005.

(29) Pinkert, D.; Demeshko, S.; Schax, F.; Braun, B.; Meyer, F.; Limberg, C. A Dinuclear Molecular Iron (II) Silicate with Two High-Spin Square-Planar FeO4 Units. *Angew. Chem. Int. Ed.* **2013**, *52*, 5155–5158.

(30) Tahsini, L.; Specht, S. E.; Lum, J. S.; Nelson, J. J. M.; Long, A. F.; Golen, J. A.; Rheingold, A. L.; Doerrer, L. H. Structural and electronic properties of old and new $A_2[M(pin^F)_2]$ complexes. *Inorg. Chem.* **2013**, *52*, 14050–14063.

(31) Pascualini, M. E.; Stoian, S. A.; Azarowski, A.; Abboud, K. A.; Veige, A. S. Solid state collapse of a high-spin square-planar Fe(II) complex, solution phase dynamics, and electronic structure characterization of an $Fe(II)_2$ dimer. *Inorg. Chem.* **2016**, *55*, 5191–5200.

(32) Ahlrichs, R.; Bär, M.; Häser, M.; Horn, H.; Kölmel, C. Electronic structure calculations on workstation computers: The program system turbomole. *Chem. Phys. Lett.* **1989**, *162*, 165–169.

(33) Dirac, P. A. M. Quantum mechanics of many-electron systems. *Proc. R. Soc. London, Ser. A* **1929**, 714–733.

(34) Slater, J. C. A simplification of the Hartree-Fock method. *Phys. Rev.* **1951**, *81*, 385.

(35) Vosko, S.; Wilk, L.; Nusair, M. Accurate spin-dependent electron liquid correlation energies for local spin density calculations: a critical analysis. *Can. J. Phys.* **1980**, *58*, 1200–1211.

(36) Becke, A. D. Density-functional exchange-energy approximation with correct asymptotic behavior. *Phys. Rev. A* **1988**, *38*, 3098.

(37) Lee, C.; Yang, W.; Parr, R. G. Development of the Colle-Salvetti correlation-energy formula into a functional of the electron density. *Phys. Rev. B* **1988**, *37*, 785.

(38) Becke, A. D. Density-functional thermochemistry. III. The role of exact exchange. *J. Chem. Phys* **1993**, *98*, 5648–5652.

(39) Weigend, F.; Furche, F.; Ahlrichs, R. Gaussian basis sets of quadruple zeta valence quality for atoms H–Kr. *J. Chem. Phys* **2003**, *119*, 12753–12762.

(40) Schäfer, A.; Huber, C.; Ahlrichs, R. Fully optimized contracted Gaussian basis sets of triple zeta valence quality for atoms Li to Kr. *J. Chem. Phys* **1994**, *100*, 5829–5835.

(41) Olson, D.; Kokotailo, G.; Lawton, S.; Meier, W. Crystal structure and structure-related properties of ZSM-5. *J. Phys. Chem.* **1981**, *85*, 2238 – 2243.

(42) Database of zeolite structures. `http://www.iza-structure.org/databases`.

(43) Andersson, K.; Malmqvist, P.-Å.; Roos, B. O. Second-order perturbation theory with a complete active space self-consistent field reference function. *J. Chem. Phys.* **1992**, *96*, 1218–1226.

(44) Aquilante, F.; De Vico, L.; Ferré, N.; Ghigo, G.; Malmqvist, P.-Å.; Neogrády, P.; Pedersen, T. B.; Pitoňák, M.; Reiher, M.; Roos, B. O. MOLCAS 7: the next generation. *J. Comput. Chem.* **2010**, *31*, 224–247.

(45) Roos, B. O.; Lindh, R.; Malmqvist, P.-Å.; Veryazov, V.; Widmark, P.-O. New relativistic ANO basis sets for transition metal atoms. *J. Phys. Chem. A* **2005**, *109*, 6575–6579.

(46) Roos, B. O.; Lindh, R.; Malmqvist, P.-Å.; Veryazov, V.; Widmark, P.-O. Main group atoms and dimers studied with a new relativistic ANO basis set. *J. Phys. Chem. A* **2004**, *108*, 2851–2858.

(47) Reiher, M.; Wolf, A. Exact decoupling of the Dirac Hamiltonian. II. The generalized Douglas–Kroll–Hess transformation up to arbitrary order. *J. Chem. Phys.* **2004**, *121*, 10945–10956.

(48) Ghigo, G.; Roos, B. O.; Malmqvist, P.-A. A modified definition of the zeroth-order Hamiltonian in multiconfigurational perturbation theory (CASPT2). *Chem. Phys. Lett.* **2004**, *396*, 142–149.

(49) Forsberg, N.; Malmqvist, P.-Å. Multiconfiguration perturbation theory with imaginary level shift. *Chem. Phys. Lett.* **1997**, *274*, 196–204.

(50) Newsam, J. M.; Treacy, M. M. J.; Koetsier, W. T.; Gruyter, C. B. D. Structural Characterization of Zeolite Beta. *Proc. R. Soc. London, Ser. A* **1988**, *420*, 375–405.

(51) Corma, A.; Navarro, M. T.; Rey, F.; Rius, J.; Valencia, S. Pure Polymorph C of Zeolite Beta Synthesized by Using Framework Isomorphous Substitution as a Structure-Directing Mechanism. *Angew. Chem. Int. Ed.* **2001**, *113*, 2337–2340.

(52) Dědeček, J.; Kaucký, D.; Wichterlová, B. Co2+ ion siting in pentasil-containing zeolites, part 3.: Co2+ ion sites and their occupation in ZSM-5: a VIS diffuse reflectance spectroscopy study. *Microporous Mesoporous Mater.* **2000**, *35–36*, 483 – 494.

(53) Dědeček, J.; Čapek, L.; Kauckỳ, D.; Sobalık, Z.; Wichterlova, B. Siting and distribution of the Co ions in beta zeolite: a UV–Vis–NIR and FTIR study. *J. Catal.* **2002**, *211*, 198–207.

(54) Kauckỳ, D.; Dědeček, J.; Wichterlová, B. Co 2+ ion siting in pentasil-containing zeolites: II. Co2+ ion sites and their occupation in ferrierite. A VIS diffuse reflectance spectroscopy study. *Microporous Mesoporous Mater.* **1999**, *31*, 75–87.

(55) Cirera, J.; Ruiz, E.; Alvarez, S. Stereochemistry and spin state in four-coordinate transition metal compounds. *Inorg. Chem.* **2008**, *47*, 2871–2889.

(56) Hu, C.; Noll, B. C.; Schulz, C. E.; Scheidt, W. R. Four-coordinate iron (II) porphyrinates: Electronic configuration change by intermolecular interaction. *Inorg. Chem.* **2007**, *46*, 619–621.

(57) Ceulemans, A.; Beyens, D.; Vanquickenborne, L. d s-mixing as a rationale for structural similarities between hexacoordinated Ni (II)-and Cu (II)-complexes. *Inorg. Chim. Acta* **1982**, *61*, 199–206.

(58) McDonald, R. G.; Hitchman, M. A. Electronic" dd" spectra of the planar tetrachlorocuprate (2-) ions in bis (methadonium) tetrachlorocuprate (II) and bis (creatininium) tetrachlorocuprate (II): analysis of the temperature dependence and vibrational fine structure. *Inorg. Chem.* **1986**, *25*, 3273–3281.

(59) Hitchman, M. A.; Bremner, J. B. The d-orbital energies in a planar nickel (II) amine complex. Evidence for 4s3d orbital mixing. *Inorg. Chim. Acta* **1978**, *27*, L61–L63.

(60) Vanquickenborne, L.; Ceulemans, A. Ligand field spectra of square-planar platinum (II) and palladium (II) complexes. *Inorg. Chem.* **1981**, *20*, 796–800.

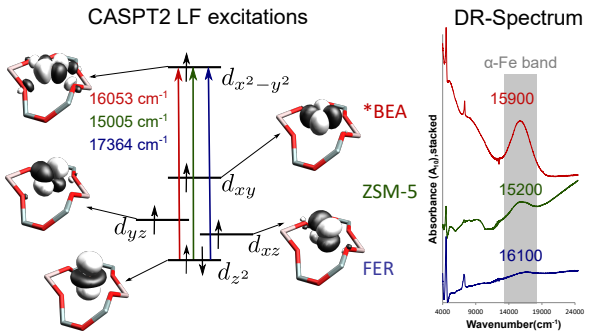

For Table of Contents Only

Table of Contents Synopsys

Fe(II) at different 6-membered ring (6MR) cation exchange sites in *BEA, ZSM-5 and FER were investigated using DFT and multirefence (CASSCF/CASPT2) methods in order to gain insight in the nature of α-Fe. These calculations demonstrate that α-Fe is a stable square planar Fe(II) species located at 6MR with a specific Al distribution. It is also shown that a significant contribution to the stability of these square planar sites is caused by Fe $3d_{z^2}4s$-mixing.